Published in final edited form as:
Phys Med Biol. 2014 March 7; 59(5): 1283–1303. doi:10.1088/0031-9155/59/5/1283.

Image-guided microbeam irradiation to brain tumour bearing mice using a carbon nanotube X-ray source array

Lei Zhang[1], **Hong Yuan**[2,3], **Laurel M Burk**[4], **Christy R Inscoe**[1,4], **Michael J Hadsell**[4], **Pavel Chtcheprov**[5], **Yueh Z Lee**[2,3,4,5,6], **Jianping Lu**[1,4], **Sha Chang**[4,5,6,7], and **Otto Zhou**[1,4,6]

Lei Zhang: leiz@email.unc.edu; Otto Zhou: zhou@email.unc.edu

[1]Department of Applied Physical Sciences, University of North Carolina at Chapel Hill, Chapel Hill, NC 27599, USA

[2]Department of Radiology, University of North Carolina at Chapel Hill, Chapel Hill, NC 27599, USA

[3]Biomedical Research Imaging Centre, University of North Carolina at Chapel Hill, Chapel Hill, NC 27599, USA

[4]Department of Physics and Astronomy, University of North Carolina at Chapel Hill, Chapel Hill, NC 27599, USA

[5]Department of Biomedical Engineering, University of North Carolina at Chapel Hill, Chapel Hill, NC 27599, USA

[6]Lineberger Comprehensive Cancer Centre, University of North Carolina at Chapel Hill, Chapel Hill, NC 27599, USA

[7]Department of Radiation Oncology, University of North Carolina at Chapel Hill, Chapel Hill, NC 27599, USA

Abstract

Microbeam radiation therapy (MRT) is a promising experimental and preclinical radiotherapy method for cancer treatment. Synchrotron based MRT experiments have shown that spatially fractionated microbeam radiation has the unique capability of preferentially eradicating tumour cells while sparing normal tissue in brain tumour bearing animal models. We recently demonstrated the feasibility of generating orthovoltage microbeam radiation with an adjustable microbeam width using a carbon nanotube based X-ray source array. Here we report the preliminary results from our efforts in developing an image guidance procedure for the targeted delivery of the narrow microbeams to the small tumour region in the mouse brain. Magnetic resonance imaging was used for tumour identification, and on-board X-ray radiography was used for imaging of landmarks without contrast agents. The two images were aligned using 2D rigid body image registration to determine the relative position of the tumour with respect to a landmark. The targeting accuracy and consistency were evaluated by first irradiating a group of mice inoculated with U87 human glioma brain tumours using the present protocol and then determining the locations of the microbeam radiation tracks using γ-H2AX immunofluorescence staining. The histology results showed that among 14 mice irradiated, 11 received the prescribed number of microbeams on the targeted tumour, with an average localization accuracy of 454 μm measured directly from the histology (537 μm if measured from the registered histological

images). Two mice received one of the three prescribed microbeams on the tumour site. One mouse was excluded from the analysis due to tissue staining errors.

1. Introduction

Radiation therapy (RT) and surgery are the most effective treatment modalities for tumour local control. Today more than half of all the cancer patients in North America rely on RT as part of their cancer management. Despite its undeniable cell killing power, RT is not always successful. This is due to the fact that the radiation dose required for tumour eradication often causes intolerable acute and/or long-term damage to surrounding normal tissue. Microbeam radiation therapy (MRT) is an experimental and preclinical radiosurgery method for cancer treatment. The technique was first developed at the Brookhaven National Laboratory (Upton, New York, USA) (Slatkin *et al* 1992, Slatkin *et al* 1995, Laissue *et al* 1998) and the European Synchrotron Radiation Facilities (Grenoble, France) (Thomlinson *et al* 2000, Laissue *et al* 1999). In this technique highly directional and high flux synchrotron radiation is spatially fractionated into quasi-parallel and microscopically thin planar X-ray beams. Synchrotron-generated X-ray microbeams are usually 25 – 75 μm in width, with centre-to-centre distances of 100 – 200 μm (Dilmanian *et al* 2003, Serduc *et al* 2009b), as illustrated in figure 1. The resulting radiation dose distribution has characteristic peaks and valleys with an extremely high peak-to-valley-dose-ratio (PVDR). A single radiation dose of up to 10^3 Gy, which is two orders of magnitude higher than what is commonly used in the accelerator based RT, is administrated within a second (Slatkin *et al* 1995). Brain tumour bearing animal model studies have shown that MRT has the unique capability of preferentially eradicating malignant tumours and extending the survival time while sparing the normal tissues irradiated by the same extremely high dose radiation. Although the normal tissue sparing and therapeutic efficacy of MRT have been demonstrated in duck embryos (Dilmanian *et al* 2001), mice (Dilmanian *et al* 2003, Miura *et al* 2006, Serduc *et al* 2006, Serduc *et al* 2008a, Serduc *et al* 2008b), rats (Slatkin *et al* 1995, Laissue *et al* 1998,Dilmanian *et al* 2002, Zhong *et al* 2003, Smilowitz *et al* 2006, Regnard *et al* 2008, Laissue *et al* 2013), and weanling piglets (Laissue *et al* 2001, Laissue *et al* 2007), this promising treatment technology has not yet been translated to the clinic.

The overall therapeutic effect of MRT is a compromise between tumour control and normal tissue sparing (Serduc *et al* 2009a). Thicker microbeams induce more tumour tissue damage, but would also increase the risk of toxicity to normal tissue (Zeman *et al* 1961, Curtis 1967, Serduc *et al* 2009a). Experimental studies have shown that normal tissue sparing effect is preserved even when using a microbeam with a beamwidth of up to several hundred microns (Dilmanian *et al* 2005, Dilmanian *et al* 2006) as long as the valley doses were kept under the threshold values, such as in the so called minibeam radiation therapy (MBRT). Also investigated at the synchrotron facilities, MBRT uses X-ray with beamwidth typically around 500 – 700 μm, about 10 times wider than the typical synchrotron MRT beam. Thicker beams are less vulnerable to beam smearing from cardio-synchronous brain tissue pulsation and will also relax the mechanical tolerance requirements for more complex MRT geometries, such like cross-hatching and interlaced cross-firing (Dilmanian *et al* 2006). Both

in vitro and in vivo studies of MBRT have shown evidence of cell killing and lifespan increase (Gil *et al* 2011, Prezado *et al* 2009, Prezado *et al* 2012).

Various theories have been proposed to explain the normal tissue-sparing and tumour cell ablation effects of MRT. Work done by Serduc *et al*. has shown the preferential effect of MRT on tumour blood vessels, leading to tumour hypoxia and eventually necrosis, while normal brain tissue vasculature exposed to MRT was found mostly undamaged and sufficiently perfused to prevent any hypoxia (Serduc *et al* 2006, Bouchet *et al* 2010, Bouchet *et al* 2013). Dilmanian *et al*., in several *in vitro* studies, showed evidence of the bystander effect for tissue restoration (Dilmanian *et al* 2007). However, there is no conclusive theory that fully explains the biology of MRT. So far all reported MRT experiments were carried out at large and high cost synchrotron facilities. Two main possible alternative radiation sources are the megavoltage LINAC and conventional orthovoltage tubes. However, the megavoltage LINAC used in conventional RT cannot be used for MRT because the large number of scattered, secondary charged particles created in the tissue would substantially increase the beam penumbra and smear out the microbeam patterns. Moreover, it has been found that extremely large peak doses (> 100 Gy) are required to completely ablate aggressive tumours for which this technique would be best-suited (Anschel *et al* 2010). Obtaining such high doses within feasible time scales is difficult using conventional orthovoltage X-ray tubes due to the anode thermal limitations. The smaller the focal spot size the lower the output power. Most conventional orthovoltage tubes have a large focal spot (usually 1-10 mm) generating a broad and divergent beam that cannot be readily used for MRT. A collimator with a narrow opening and very large aspect ratio is needed to collimate the intrinsically divergent beam to obtain the desired microbeam pattern with efficiently high PVDR. In this geometry X-ray photons originated from most of the focal area do not pass through the microbeam collimator and the actual microbeam dose rate delivered is largely reduced. Although micro-focused orthovoltage X-ray tubes are commercially available, they operate at much lower power. In contrast to its alternatives, synchrotron generated X-ray radiation has minimal angular divergence and therefore can be readily collimated into parallel micro-planar beams. Ultra-high dose rates allow for instantaneous delivery of high doses to maintain the microbeam profile despite physiological motion. The reliance on synchrotron radiation, however, has hindered more widespread research on this promising approach for cancer treatment and is a major roadblock for translation into clinical applications.

We recently developed a spatially distributed X-ray source array technology using the carbon nanotube (CNT) field emitters as a “cold cathode” (Zhou and Lu 2003, Zhang *et al* 2005, Zhou and Calderon-Colon 2010). The CNT cathode emits an electron beam under an applied electric field, which is then accelerated to bombard the metal anode to generate X-rays. Compared to a conventional thermionic X-ray tube, where the radiation is generated from a single focal point on the anode, the field emission technology affords greater flexibility in the source design in terms of the dimension, number of sources, geometric configuration of the individual source, and the mode of operation. By sequentially switching on and off the individual and spatially distributed sources, a “scanning” X-ray beam can be generated to image an object from different viewing angles without mechanical motion,

which enables fast and high-resolution tomography imaging. This has been demonstrated in stationary digital tomosynthesis for imaging the breast (Qian *et al* 2012) and chest (Shan *et al* 2013), tomosynthesis-guided radiation therapy (Maltz *et al* 2009), and stationary computed tomography (Gonzales *et al* 2013). To obtain a higher X-ray flux, all or a subset of the X-ray sources can be switched on at the same time to irradiate an object from different directions. The field emission X-ray source can be electronically switched on and off by controlling the emission current from the CNT cathode, and can be readily gated with physiological signals for prospective imaging (Cao *et al* 2009, Cao *et al* 2010).

Utilizing the unique capabilities of the CNT X-ray source array technology we recently demonstrated the feasibility of generating orthovoltage microbeam radiation (Zhou and Chang 2010, Schreiber and Chang 2012, Hadsell *et al* 2013). The prototype device utilized a specially designed CNT X-ray source array with a long and narrow focal track to deliver the radiation simultaneously from different directions, instead of from a single point, to the region of interest. An external collimator was used to collimate the radiation into a microbeam of adjustable beamwidth. A higher dose rate was achieved by distributing the electron energy over the long focal tracks with increased heat capacity compared to conventional point-focus X-ray tubes. The electronically controlled field emission of the electrons and resultant X-ray generation enabled accurate and reliable delivery of the radiation, and also allowed for physiologically gated irradiation which minimizes motion-induced blurring of the microbeam pattern (Chtcheprov *et al* 2013). Minimal motion-induced blurring is critical for non-synchrotron based MRT with an inevitably longer treatment time. The irradiator was integrated with a CNT-based micro-CT scanner (Cao *et al* 2010) for image guidance. To increase the treatment throughput, special mouse beds were designed to allow irradiation of two mice simultaneously, with independent anaesthesia and physiological monitoring capabilities. At full power, this first generation system can deliver an instantaneous dose rate of 2 Gy/s at the entrance plane with a PVDR of over 17 (Hadsell *et al* 2013).

The goal of this study is to evaluate an image-guidance protocol for targeted delivery of microbeam radiation to mouse brain tumours. Because tumours are usually located deep inside the mouse brain, and small in size (~2 mm in diameter), it is technically challenging to accurately align the narrow microbeams with the small tumour volume. X-ray and CT imaging can quickly capture bone structures but are not ideal for brain tumour imaging due to low soft tissue contrast, even with a considerable dose of contrast agent. Contrast agent increases toxicity risk to the animal and complicates the treatment outcomes. Magnetic resonance imaging (MRI) provides good tumour tissue contrast non-invasively, but needs to be performed at a separate location. Throughout the course of this study we investigated a hybrid image-guidance protocol that combines MRI with on-board 2D X-ray radiography in order to identify the tumour location with respect to the microbeam position, to ensure accurate dose delivery. We evaluated the accuracy and consistency of this protocol using brain tumour mouse models and characterized the cell responses to radiation using γ-H2AX immunofluorescence staining. Stained tissue slices produced clear patterns of tissues' DNA damage corresponding to the microbeam path and spatial arrangements, which were used to estimate the targeting accuracy.

2. Methods and materials

2.1. The compact image-guided MRT system

As shown in figure 2, the prototype image-guided MRT system consists of a CNT field emission X-ray source array irradiator and a high-resolution micro-CT scanner. The X-ray irradiator consists of a linear CNT field emission cathode array, which emits electrons under a biased extraction field, an electrostatic focusing lens and an opposing stationary tungsten anode. The electron beam is focused down to a narrow focal line on the reflective anode measuring approximately 0.142 mm in width and 160 mm in length after projection at an angle of 8°. The X-ray source array is operated at 160 kVp anode voltage and 30 mA tube current. The intrinsically divergent line of radiation is collimated into a microbeam using a motorized slit collimator placed between the X-ray window and the object, as shown in figure 3. Parallel planes of microbeam irradiation are generated by translating the object in the direction perpendicular to the microbeam plane in a step-and-shoot fashion. For this study, a 280 μm wide (determined via film measurements at the entrance plane during tube dosimetric characterization) microbeam was used.

The homemade micro-CT scanner is composed of a micro-focused CNT field emission X-ray source (XinRay Systems Inc., NC) with an effective focal spot size of 100 μm × 100 μm, and an operating anode voltage of up to 50 kVp. In addition, the system contains a 5 cm × 5 cm flat panel detector (Hamamatsu C7921CA-02), with a pixel size of 50 μm × 50 μm, mounted on a rotating gantry (Cao *et al* 2010). The isocentre of the micro-CT scanner is aligned with the irradiator's microbeam entrance location on the mouse head. Two customized mouse holders were fabricated by 3D printing as shown in figure 4. The holders were designed to accommodate the head-immobilizing hardware, the anaesthesia tubing and the respiration sensor. The head-immobilizing hardware consists of two ear bars that can be fastened securely to hold the mouse head in a non-rotated and non-tilted position in order to achieve accurate image registration with MRI. The nose cone holds the isoflurane-in and exhaust-out tubing in place, and supports the mouse head at a proper height. The respiration rate was monitored by the pressure sensor underneath the abdomen of the mouse, from which the signals were visualized and recorded on the *Biovet* (m2m Imaging Corp., OH) user interface throughout the entire procedure. High precision translation stages (Velmex Inc., NY) transport the animals from the imaging site to the irradiation location. The stages (Velmex Inc., NY) have a line accuracy of 76 μm. The actuators (Newport Corp., CA), used for adjusting the relative positions of the two mouse beds, have on-axis accuracy of ~ 10 μm.

2.2. Dosimetry

Dosimetry of this compact MRT prototype was performed using Gafchromic EBT2 film (Ashland Advanced Materials, Covington, KY, US) calibrated to an ion chamber (RadCalTM 10X5-0.6CT Farmer-type, with a MDH-1015C control unit. The Gafchromic EBT2 film was chosen due to its weak energy dependence in the 60 keV to MeV range (Arjomandy et al 2010), high sensitivity in the 0 - 100 Gy dose range, and high spatial resolution (Andres et al 2010). The film was calibrated by benchmarking the measured output of the ion chamber irradiated in the uncollimated beam to the response of the film

under the same conditions. Eleven film swatches were irradiated with doses ranging from 0-56 Gy as measured by the ion chamber. These films were scanned using a Perfection V700 flatbed scanner (Epson America, Long Beach, CA) in 48-bit color and 72 dpi. Finally, the raw scanner response values for all three color channels were fitted to the known dose values using a rational function as recommended by Ashland, Inc. (Hadsell 2013).

The dose rate at the typical source to surface distance of 124 mm for our in-vivo experiments was determined based upon Gafchromic EBT2 film measurement as well. These measurements were performed by irradiating EBT2 film with several microbeams delivered using various beam-on times, all using the same machine settings presented in this work. The film was scanned at 2400 dpi, and the peak dose for each microbeam was measured using single channel (green) dosimetry in *FilmQAPro* (Ashland Advanced Materials, Covington, KY US). The peak doses were then plotted against the beam-on time used for each microbeam and fit by a linear regression. The average dose rate was found to be 1.16 Gy/min at 124 mm from the focal line, with the tube operating at 8% duty cycle (Hadsell 2013). Based on this value, the dose rate exiting the microbeam collimator was then extrapolated using previously measured tissue maximum ratio (TMR) and distance correction tables to be 2.42 Gy/min.

For this study, *Gafchromic* EBT2 films were placed at the entrance and exit planes of the mouse head during the radiation to qualitatively verify the gross positioning of the mouse and proper beam delivery. All films were scanned in 48-bit color and at 2400 dpi using the same V700 scanner according to the recommended handling procedures of Ashland, Inc. The film scans were then analyzed using the calibration curves described above and multi-channel film dosimetry (Micke *et al* 2011, van Hoof *et al* 2012) as implemented by *FilmQAPro*. Due to the upper limit of our calibration curve, only those verification films from treatment plans with dose levels within the 0 – 60 Gy range were scanned and analyzed to create dose profiles. These dose profiles were then compared with the prescribed treatment plans, i.e. verifying expected peak dose, beam width, and beam separation.

2.3. Mouse model and mouse handling

Experimental procedures carried out in this study were approved by the Institutional Animal Care and Use Committee at our institution. Fourteen young adult (4 - 6 weeks old), male, athymic nude mice were used for this tumour-targeting MRT experiment. U87MG human glioma tumour cells were cultured in Dulbecco's Modified Eagle's Medium (DMEM) plus 1% Fetal Bovine Serum (FBS) before being collected for injection. Three weeks before irradiation, and with stereotactical guidance, 2×10^5 cells in 5 μl serum-free medium were injected intracranially into the right forebrain — 1mm anterior, 2.5 mm lateral, and 4 mm down to the bregma — to induce brain tumour growth in the mouse. For all imaging and MRT treatment procedures, the mice were anesthetized with 1% - 2.5% isoflurane in medical-grade oxygen at 0.8 or 1 L/min flow rate.

2.4. MR and X-ray imaging

The image-guided MRT protocol is outlined in chart 1. One day before radiation treatment, mice were brought to the imaging facility (Biomedical Research Imaging Centre, UNC-

Chapel Hill) for MRI with a 9.4 Tesla MR scanner (Bruker BioSpin, Inc. Billerica, MA). T2-weighted images were acquired using a Rapid Acquisition with Refocused Echoes (RARE) sequence with an echo spacing-to-recovery time ratio (TE/TR) of 22/3406, 256 × 256 matrix size, 0.5 mm slice thickness, and 100 micron sagittal and coronal in-plane resolution. The tumours ranged in diameter from 1.5 mm to 2.1 mm were delineated in T2w images with hyper-intense signal. The MR images used for registration were created from the sagittal images. The central three slices near the brain midline were averaged to form a sagittal projection image. This projection was later used to align with the sagittal X-ray projection of the same mouse. The tumour location was projected to the centre slice.

After MRI, the mice were transported to the MRT lab on the day of irradiation. While under anaesthesia, the mice were first immobilized in the prone position on the customized holders. The ear bars, nose cone and the teeth clamping altogether ensured immobility of the sedated mice. Two mice were immobilized on two separate mouse beds, which were then mounted side by side on translation stage (figure 5 top). X-ray projections of the two mice were taken using the micro-CT scanner at 45 kVp and 0.024 mAs per projection. Imaging of the mice was performed one at a time in an image-and-shift manner, as illustrated in figure 5 (middle and bottom). The actuator and micrometer attached to the mouse bed positioned the head of the mouse being imaged at the centre of the detector field of view, while the other mouse was kept outside of the X-ray beam pathway. X-ray projections were acquired from the same orientation (sagittal view) as that in the MRI. Afterwards the mouse imaged first was shifted out from the field of view; the other was moved in, and imaged in the same manner. The projections were corrected with dark and blank images using a *MATLAB* (MathWorks Inc., Natick, Massachusetts, US) program. For X-ray imaging, the ear bars on the mouse holder were used as the fiducial landmarks because they were easily calibrated to both the microbeam position and the brain structures of the mouse.

2.5. Image registration

The sagittal MR images and corrected X-ray images were scaled to the same pixel size, and aligned manually using *Photoshop* (Adobe Systems Inc., San Jose, California U.S.) and *ImageJ* (Public Domain, Developed by Wayner Rasband, NIH) using rigid-body registration method. Skull contours were identified on both MR and X-ray images, and then aligned together. Once the images were registered, the relative distance from the tumour centre to the ear bars, Δx_1, was calculated from the registered images in both anterior-posterior and superior-inferior directions, as shown in figure 6. Since the two ear bars may not be concentric in the projection images depending on their location in the image and the differences in magnification, the midpoints of two ear bars were averaged and used as the ‘centre of ear bar’. The microbeam planes transversely intersect with the mouse brain at a slight angle of 8 degrees (collimator angle), as shown in figure 7 on the left.

2.6. Microbeam alignment and irradiation

Figure 6 shows the geometrical parameters that need to be determined in order to accurately deliver the microbeam to the tumour. Since the planar microbeams are delivered in the y-z plane and no conformal collimation is used in the current setup, only the relative distances in the x direction are needed. To determine the microbeam entrance position with respect to the

ear bars, a piece of *Gafchromic* film was placed on the top surface of the mouse holder, and translated into the MRT chamber with the travel distance, Δx_2, being recorded. A low dose single microbeam was delivered on the film for calibration purposes. The distance between the centre of the microbeam to the 'centre of ear bars', Δx_3, was measured with the use of a pair of calipers. Using the tumour location relative to the ear bars, Δx_1, determined from registration, the distance between the tumour and the microbeam entrance point for the mice pair was therefore calculated by the summation of Δx_1, Δx_2, and Δx_3, with the signs assigned accordingly.

After imaging, the mice were translated from the imaging location to the irradiation site, ready for treatment. The number of microbeams, beam pitch, and the beam delivery locations on the tumour site, were decided based on the registered image and tumour size. For this targeting study, we chose various dose levels and different numbers of microbeams for the animals (as assigned below), which was also investigated in another study for cellular responses. The microbeam irradiator was running at a constant anode voltage of 160 kV, producing a microbeam of 280 μm full-width-half-maximum (FWHM) at the animal head entrance plane. The average dose rate at the entrance plane was 1.16 Gy/min, determined as noted before. In total, fourteen tumour bearing mice were irradiated in seven groups, two mice at a time following the procedures described above, as shown in figure 7.

The first pair of mice was irradiated by a single microbeam of 138 Gy entrance dose, targeted at the centre of the tumour. The second pair of mice was irradiated by two parallel microbeams with centre-to-centre distance of 900 μm. A 900 μm centre-to-centre distance was chosen to maintain a relatively high PVDR with 280 μm beamwidth, and to achieve good coverage of the tumour area. The prescribed entrance dose for each microbeam was about 108 Gy. Between the two microbeams, the first was targeted at the centre of the tumour while the second was targeted 900 μm away. The remaining 5 pairs of mice were irradiated by three microbeams, with a 900 μm pitch, delivering 48 Gy at the entrance of each microbeam.

2.7. Immunohistological confirmation

To evaluate the targeting accuracy and the tumour cell response, γ-H2AX immunofluorescence staining was used as a quantitative biomarker of radiation-induced DNA double-strand breaks (DSB). This process confirms the delivery of microbeams through the tumour tissue sections post irradiation. The mice were euthanized at various time points (1 hr, 4 hrs, 24 hrs, 48 hrs, and 7 days) post-MRT. Their brains were collected and fixed in formalin. The fixed brains were cut in half along the midline and embedded in paraffin. Before tissue sectioning, the distance between the centre midline to the targeted tumour plane in the sagittal view that was used for treatment planning was first measured from both coronal and sagittal MR images. This distance was then used in sectioning to determine the tumour location on the paraffin-embedded brain hemisphere, taking into account a 20% shrinkage rate from the dehydration process (Winsor 1994). Ten, 5 μm sections were cut in the sagittal plane, perpendicular to the microbeams, near the target locations. One of the sections was used for γ-H2AX staining. The staining procedures followed the published protocol (Crosbie *et al* 2010). Briefly, the tissue section was de-

paraffinated, rehydrated, antigen-demasked by citrate buffer, and then incubated with the primary antibody (Phosphohistone H2AX Rabbit anti-mouse antibody, Cell Signaling Technology Inc.) for 60 min. This was followed by incubation with the secondary antibody with Cy5 Tyramide and DAPI counter-staining on the nuclei. The section was then scanned using a fluorescence slide scanner system (Scanscope FL scanner, Aperio Inc., Vista, CA) to obtain a whole brain slide image.

3. Results

3.1. MR and X-ray images and registration

A typical set of MR, X-ray projection and registered images is shown in figure 8. The 2-D shape, size and location of the tumour can be clearly visualized in the MR image. The average tumour size was measured to be approximately 1.4×2.2 mm^2 on the sagittal plane, with the tumour centre marked out. In the corrected X-ray projection, the primary bone structures including the skull features, jaw, and spinal cord, the ear bars and the anaesthesia tubing on the mouse holders were well displayed. The registered image combined information from both the MR and X-ray images, showing both the tumour and the ear bars. From the registered image, the relative distance along the x-axis between the centre of the tumour and the ear bars was measured.

3.2. Verification of beam delivery

Gafchromic films were placed at the entrance and exit planes of mouse head for qualitative verification of beam delivery. All films were scanned in 48-bit color and at 2400 dpi using the V700 scanner following the handling procedures recommended by Ashland, Inc. Number of beams and c-t-c distances were confirmed in all films to be consistent with the prescription. The films irradiated by planned doses that fell into 0 - 60 Gy dose range were analyzed using triple channel dosimetry in *FilmQAPro*. Figure 9 shows the results of the analyzed films from a tumour mouse treated with three microbeams with dose of 48 Gy/beam. The FWHM of the dose profile was measured to be 280 μm at the entrance plane, which was consistent with our tube calibration results. The beam width broadened to 380 μm at the exit plane underneath the mouse skull. The measured peak dose of each beam was consistent with the prescribed value as well. The PVDR was calculated as,

$$PVDR = \frac{D_{peak}}{D_{valley}} \quad (1)$$

D_{peak} and D_{valley} are the average doses measured at the centre of peak, and the centre of valley respectively. The average PVDR was calculated to be 16 +/-1 at the entrance plane, and reduced to 14 +/-1 at the exit plane.

3.3. Immunohistological confirmation

Figure 10 shows the γ-H2AX stained images of the irradiated mouse brain slices. The γ-H2AX foci-positive cells shown as pink strips were clearly visible in the stained sections indicating radiation-induced DNA double-strand breaks. These patterns corresponded to the microbeam path and spatial arrangements through the tumour and normal tissues. The

geometric centre-to-centre distance between two adjacent tracks was measured to be 800 μm, which matches with the prescribed beam pitch of 900 μm when taking into account the average 20% anisotropic shrinkage rate (Winsor 1994) of the paraffin embedded slice.

The targeting error was first evaluated directly from the stained sagittal sections by measuring the horizontal displacement, Δx, from the centre of the microbeam to the centre of the tumour. Out of the 14 animals in this study, one animal was excluded due to cutting and staining mistakes. The average horizontal displacement Δx of the remaining 13 mice was approximately 454 μm. The values measured via this manner are listed in column 2 of table 1.

Since the MR images were taken the day before MRT and the animals were euthanized at different time points post MRT, there might have been anisotropic tumour growth between the MRI and euthanization. This created difficulties in identifying the original target centre in the stained section. The targeting accuracy was also evaluated by manually registering γ-H2AX stained image back to the corresponding pre-treatment MR sagittal images, as shown in figure 1. The γ-H2AX stained image recorded the microbeams' positions while the MR sagittal image showed the original targeted tumour centre. This alignment method is similar to the X-ray/MR image registration mentioned previously in this paper, except that here we used features in the brain and cerebellum instead of skull contour for alignment. The targeting errors Δx measured in this way are listed in column 3 of table 1.

4. Discussion and conclusions

In total, 14 animals were irradiated using the combined X-ray/MRI image-guided MRT protocol described above. Due to tissue sectioning and staining errors, one mouse was excluded from the analysis. The histology data showed that 11 out of the remaining 13 animals successfully received all of the prescribed number of microbeams on the targeted tumours. The other two mice received one out of the three planned microbeams at the primary tumour site while the other 2 microbeams were delivered outside the targeted tumour location. One of these two mice with misplaced microbeams had a relatively small tumour size (<1.4 mm) along the beam array direction, considering the centre-to-centre spacing used in this study was 900 μm. It is noticed that one of the two mice (Animal ID 1086), which was irradiated with a single high dose microbeam, showed a relatively high error (in both error calculation methods) compared to the rest of the mice. The respiratory pattern recorded by the *Biovet* monitoring program indicated that this animal experienced multiple substantial gasps during the irradiation. This could have caused body movement or loosening of the ear bars, leading to the reduced targeting accuracy for this specific animal. Regardless, the results for these two mice were included in the estimation of the targeting error.

There are several potential sources of error in the present procedure including uncertainties in the registration of MR and X-ray images, and consistency in positioning the mouse. First of all, since MR and X-ray images were taken at different facilities, there were transportation and re-positioning of animal from one facility to another. Even though immobilized using the same type of mouse holders and imaged from the same direction, the

animals were not positioned exactly the same for MR and X-ray imaging. The variations in orientation of the mouse eventually led to variations in the images. Secondly, the features used for image matching were not perfectly sharp and the images were collected at a finite resolution, both of which contributed to the targeting error observed in this study. Besides, the large tissue shrinkage and deformation not only made it hard to manually align the stained tissue section to the MR image, but it also degraded the accuracy of any measurement from the stained slice.

Another source of uncertainty comes from the mouse head immobilization and anaesthesia during irradiation. In our customized mouse holder design, the teeth clamping wire, nose cone, and the ear bars altogether should provide sufficient immobility during irradiation providing that the animals were put under anaesthesia. However, if the animal experienced substantial gasping during RT, such as what has happened to mouse ID 1086, drastic body motion or even loosening of the ear bars and teeth clamp could lead to animal dislocation and microbeam being delivered off-target.

The microbeam delivery accuracy obtained in the present study is comparable with the targeting accuracy reported in the literature for image-guided small animal irradiators (Verhaegen *et al* 2011). Matinfar *et al.* showed an error of 0.2 mm in beam alignment when irradiating a radio-opaque marker in a rigid phantom using an in-house small animal radiation research platform (SARRP) (Matinfar *et al* 2009), and an average displacement in mouse repositioning of 0.8 +/− 0.49 mm using this system was reported in a separate study (Armour *et al* 2010). Another commercially available small animal irradiation device, X-Rad 225Cx (PXI, North Branford, CT) claimed an image-guidance accuracy of no larger than 0.5 mm, and the study on this device by Clarkson *et al*. concluded a consistent accuracy on the order of 0.2 mm in targeting the centre of a metal BB fixed to radiochromic film (Clarkson *et al* 2010). The small animal research system adapted from a micro-CT at Stanford University achieved 0.1 mm accuracy in each direction using a solid water phantom containing a metal sphere (Zhou *et al* 2010). A distinction must be made when comparing the image-guidance performance of our system to other small animal IGRT systems is the target objects used in the evaluation. In this study, the accuracy level was quantified *in vivo* – targeting the mouse brain tumour which usually has no well-defined structure and no sharp, clear edges, whereas in other systems it was evaluated using rigid phantoms with unambiguous margins. In addition to the higher requirement in image quality for brain tumour visualization, the respiration-induced brain motion in the animal during imaging and irradiation posed more challenges for our evaluations compared to rigid phantom studies. On the other hand, all other preclinical IGRT systems generally operate at too large of a field size with large beam penumbras, making them not suitable for MRT. For example, the smallest field size that the SARRP can produce is 500 μm, at which the system can only provide a dose rate of up to 22 cGy/min at 1 cm depth in water (Wong *et al* 2008). And even then, the 20-80% penumbra is almost 0.2 mm on each side (Wong *et al* 2008). So far, the system presented in this study is the only one capable of generating microbeams of relevantly high dose rate for small animal studies (Verhaegen *et a*l 2011), with a PVDR well within the range of Synchrotron MRT (Anschel *et al* 2010).

On-board image guidance was not implemented in most of the synchrotron MRT experiments. To ensure tumour coverage the conformal microbeam radiation delivered typically covers a much larger area (typically in the order of 10 mm × 10 mm) than the size of the brain tumour, by mechanically scanning the mouse mounted on a precision goniometer through the microbeam arrays in a fraction of a second. For such size irradiation fields, Laissue *et al*. estimated that the ratio of the tumour volume to the total brain volume covered by microbeam arrays was only about 0.06, and therefore a very large amount of normal brain was enclosed in the target volume where the heaviest damage was seen (Laissue *et al* 1998). Planar X-ray imaging was utilized in several recent studies to either identify the tumour cell injection point (Romanelli *et al* 2013) or to locate specific skull landmarks for homogenous irradiation of brain regions (Serduc *et al* 2010) without direct localization of the actual tumour to be treated. This is because planar X-ray by itself cannot readily visualize brain tumour without using high concentration of X-ray contrast agent due to the limited tumour contrast, which may cause toxicity and contaminate the treatment result. For this reason MR was used in this study to identify the tumour in addition to on-board planar X-ray imaging.

Accurately delivering the microbeams to the targeted tumour site is necessary for the present compact MRT device. The low dose rate makes it essential to confine the radiation area to the tumour in order to minimize the total irradiation time. The results reported here demonstrate that this can be accomplished using the presented combined MRI/X-ray image guidance procedure. In the preliminary study, 11 out of the 13 analyzed animals received all the prescribed microbeams on the targeted small brain tumours. Only two mice had microbeams misplaced outside the tumour region. There remains much room for improvement in this protocol, i.e. the microbeam alignment, animal fixation, image registration and staining procedures, which would all contribute to a better targeting accuracy. An affine registration algorithm for the brain histology section and MR image alignment can potentially be implemented to provide more accurate evaluation of the targeting errors. Also, if one mouse is irradiated at a time instead of two, CT images of the mouse can be collected using the on-board micro-CT scanner for 3D registration with the MRI to improve the registration accuracy.

Although still at a very early stage of the development, the present study demonstrates the feasibility of image-guided microbeam irradiation using distributed carbon nanotube X-ray source array technology. Targeted microbeam radiation with the energy, beam width, and peak-valley-dose-ratio within the range considered necessary for the therapeutic effects observed in the synchrotron MRT studies has been generated and delivered to live mice. One limitation of the present first generation system is that its average dose rate is still too low to deliver the high peak entrance dose considered necessary for tumour eradication within the biologically reasonable time window of the mouse model. A second-generation nanotube X-ray based microbeam irradiator is currently under construction, which will provide a factor of 20 increase in the average dose rate over the present system. This will enable targeted delivery of microbeams with peak dose matching the lower end of values used in the synchrotron MRT studies.

Acknowledgments

This work is supported by the National Cancer Institute (NCI) funded Carolina Centre for Cancer Nanotechnology Excellence (U54-CA151652) and the NCI Grand Opportunity grant (RC2-CA148487). We would like to thank Dr. Ryan Miller's lab at UNC Department of Pathology for providing the tumour cells, UNC Translational Pathology Laboratory and Jon Frank from UNC BRIC for helping with animal handling, and Dr. Joel Tepper at UNC Radiation Oncology for helpful discussions.

References

Andres C, del Castillo A, Tortosa R, Alonso D, Barquero R. A comprehensive study of the Gafchromic EBT2 radiochromic film: A comparison with EBT. Med Phys. 2010; 37:6271–8. [PubMed: 21302783]

Anschel DJ, Bravin A, Romanelli P. Microbeam radiosurgery using synchrotron-generated submillimetric beams: a new tool for the treatment of brain disorders. Neurosurg Rev. 2010; 34:133–42. [PubMed: 21088863]

Arjomandy B, Tailor R, Anand A, Sahoo N, Gillin M, Prado K, Vicic M. Energy dependence and dose response of Gafchromic EBT2 film over a wide range of photon, electron, and proton beam energies. Med Phys. 2010; 37:1942–7. [PubMed: 20527528]

Armour M, Ford E, Iordachita I, Wong J. CT guidance is needed to achieve reproducible positioning of the mouse head for repeat precision cranial irradiation. Radiat Res. 2010; 173:119–23. [PubMed: 20041766]

Bouchet A, et al. Synchrotron microbeam radiation therapy induces hypoxia in intracerebral gliosarcoma but not in the normal brain. Radiother Oncol. 2013; 108:143–8. [PubMed: 23731617]

Bouchet A, et al. Preferential effect of synchrotron microbeam radiation therapy on intracerebral 9L gliosarcoma vascular networks. Int J Radiat Oncol Biol Phys. 2010; 78:1503–12. [PubMed: 20932689]

Cao G, et al. A dynamic micro-CT scanner based on a carbon nanotube field emission x-ray source. Phys Med Biol. 2009; 54:2323–40. [PubMed: 19321922]

Cao GH, Burk LM, Lee YZ, Calderon-Colon X, Sultana S, Lu JP, Zhou O. Prospective-gated cardiac micro-CT imaging of free-breathing mice using carbon nanotube field emission x-ray. Med Phys. 2010; 37:5306–12. [PubMed: 21089765]

Chtcheprov, P.; Hadsell, M.; Burk, L.; Ger, R.; Zhang, L.; Yuan, H.; Lee, YZ.; Chang, S.; Lu, J.; Zhou, O. Physiologically gated micro-beam radiation therapy using electronically controlled field emission x-ray source array. In: Holmes, DR.; Yaniv, ZR., editors. Proc SPIE Medical Imaging Conference; Lake Buena Vista (Orlando Area), Florida USA. 2013. p. 86711Z

Clarkson R, Lindsay PE, Ansell S, Wilson G, Jelveh S, Hill RP, Jaffray DA. Characterization of image quality and image-guidance performance of a preclinical microirradiator. Med Phys. 2011; 38:845–56. [PubMed: 21452722]

Crosbie JC, et al. Tumor cell response to synchrotron microbeam radiation therapy differs markedly from cells in normal tissues. Int J Radiat Oncol Biol Phys. 2010; 77:886–94. [PubMed: 20510199]

Curtis HJ. The Use of a Deuteron Microbeam for Simulating the Biological Effects of Heavy Cosmic-Ray Particles. Radiat Res Suppl. 1967; 7:250–7. [PubMed: 6058661]

Dilmanian FA, et al. Response of rat intracranial 9L gliosarcoma to microbeam radiation therapy. Neuro Oncol. 2002; 4:26–38. [PubMed: 11772430]

Dilmanian FA, et al. Response of avian embryonic brain to spatially segmented x-ray microbeams. Cell Mol Biol. 2001; 47:485–93. [PubMed: 11441956]

Dilmanian FA, Morris GM, Zhong N, Bacarian T, Hainfeld JF, Kalef-Ezra J, Brewington LJ, Tammam J, Rosen EM. Murine EMT-6 carcinoma: high therapeutic efficacy of microbeam radiation therapy. Radiat Res. 2003; 159:632–41. [PubMed: 12710874]

Dilmanian FA, Qu Y, Feinendegen LE, Pena LA, Bacarian T, Henn FA, Kalef-Ezra J, Liu S, Zhong Z, McDonald JW. Tissue-sparing effect of x-ray microplanar beams particularly in the CNS: is a bystander effect involved? Exp Hematol. 2007; 35:69–77. [PubMed: 17379090]

Dilmanian FA, et al. X-ray microbeams: Tumor therapy and central nervous system research. Nucl Instrum Methods Phys Res A. 2005; 548:30–7. [PubMed: 17369874]

Dilmanian FA, Zhong Z, Bacarian T, Benveniste H, Romanelli P, Wang R, Welwart J, Yuasa T, Rosen EM, Anschel DJ. Interlaced x-ray microplanar beams: a radiosurgery approach with clinical potential. Proc Natl Acad Sci USA. 2006; 103:9709–14. [PubMed: 16760251]

Gil S, Sarun S, Biete A, Prezado Y, Sabes M. Survival analysis of F98 glioma rat cells following minibeam or broad-beam synchrotron radiation therapy. Radiat Oncol. 2011; 6

Gonzales, B.; Spronk, D.; Cheng, Y.; Zhang, Z.; Pan, X.; Beckmann, M.; Zhou, O.; Lu, J. Rectangular computed tomography using a stationary array of CNT emitters: initial experimental results. In: Nashikawa, RM.; Whiting, BR., editors. Proc SPIE Medical Imaging Conference; Lake Buena Vista (Orlando Area), Florida USA. 2013. p. 86685K

Hadsell, M. Ph D Thesis. University of North Carolina; Chapel Hill: 2013. The development and characterization of a first generation carbon nanotube x-ray based microbeam radiation therapy system; p. 196-254.

Hadsell M, Zhang J, Laganis P, Sprenger F, Shan J, Zhang L, Burk L, Yuan H, Chang S, Lu J, Zhou O. A first generation compact microbeam radiation therapy system based on carbon nanotube X-ray technology. Appl Phys Lett. 2013; 103:183505. [PubMed: 24273330]

Laissue JA, et al. Response of the rat spinal cord to X-ray microbeams. Radiother Oncol. 2013; 106:106–11. [PubMed: 23321495]

Laissue, JA.; Blattmann, H.; Di Michiel, M.; Slatkin, DN.; Lyubimova, N.; Guzman, R.; Zimmermann, W.; Birrer, S.; Bley, T.; Kircher, P. Proc SPIE. Vol. 4508. San Diego, CA USA: 2001. Weanling piglet cerebellum: a surrogate for tolerance to MRT (microbeam radiation therapy) in pediatric neuro-oncology; p. 65-73.

Laissue JA, Blattmann H, Wagner HP, Grotzer MA, Slatkin DN. Prospects for microbeam radiation therapy of brain tumours in children to reduce neurological sequelae. Dev Med Child Neurol. 2007; 49:577–81. [PubMed: 17635201]

Laissue JA, et al. Neuropathology of ablation of rat gliosarcomas and contiguous brain tissues using a microplanar beam of synchrotron-wiggler-generated X rays. Int J Cancer. 1998; 78:654–60. [PubMed: 9808538]

Laissue, JA.; Lyubimova, N.; Wagner, H-P.; Archer, DW.; Slatkin, DN.; Di Michiel, M.; Nemoz, C.; Renier, M.; Brauer, E.; Spanne, PO. Proc SPIE. Vol. 3770. Denver, CO USA: 1999. Microbeam radiation therapy; p. 38-45.

Maltz JS, Sprenger F, Fuerst J, Paidi A, Fadler F, Bani-Hashemi AR. Fixed gantry tomosynthesis system for radiation therapy image guidance based on a multiple source x-ray tube with carbon nanotube cathodes. Med Phys. 2009; 36:1624–36. [PubMed: 19544779]

Matinfar M, Ford E, Iordachita I, Wong J, Kazanzides P. Image-guided small animal radiation research platform: calibration of treatment beam alignment. Phys Med Biol. 2009; 54:891–905. [PubMed: 19141881]

Micke A, Lewis FD, Yu X. Multichannel film dosimetry with nonuniformity correction. Med Phys. 2011; 38:2523–34. [PubMed: 21776787]

Miura M, Blattmann H, Brauer-Krisch E, Bravin A, Hanson AL, Nawrocky MM, Micca PL, Slatkin DN, Laissue JA. Radiosurgical palliation of aggressive murine SCCVII squamous cell carcinomas using synchrotron-generated X-ray microbeams. Br J Radiol. 2006; 79:71–5. [PubMed: 16421408]

Prezado, Y.; Renier, M.; Bravin, A. Proc IFMBE. Vol. 25. Munich, Germany: 2009. A new synchrotron radiotherapy technique with future clinical potential: minibeams radiation therapy; p. 29-32.

Prezado Y, Sarun S, Gil S, Deman P, Bouchet A, Le Duc G. Increase of lifespan for glioma-bearing rats by using minibeam radiation therapy. J Synchrotron Radiat. 2012; 19:60–5. [PubMed: 22186645]

Qian X, Tucker A, Gidcumb E, Shan J, Yang G, Calderon-Colon X, Sultana S, Lu J, Zhou O, Spronk D. High resolution stationary digital breast tomosynthesis using distributed carbon nanotube x-ray source array. Med Phys. 2012; 39:2090. [PubMed: 22482630]

Regnard P, et al. Irradiation of intracerebral 9L gliosarcoma by a single array of microplanar x-ray beams from a synchrotron: balance between curing and sparing. Phys Med Biol. 2008; 53:861–78. [PubMed: 18263945]

Romanelli P, et al. Synchrotron-generated microbeam sensorimotor cortex transections induce seizure control without disruption of neurological functions. PLoS One. 2013; 8:e53549. [PubMed: 23341950]

Schreiber EC, Chang SX. Monte Carlo simulation of a compact microbeam radiotherapy system based on carbon nanotube field emission technology. Med Phys. 2012; 39:4669–78. [PubMed: 22894391]

Serduc R, Berruyer G, Brochard T, Renier M, Nemoz C. In vivo pink-beam imaging and fast alignment procedure for rat brain lesion microbeam radiation therapy. J Synchrotron Radiat. 2010; 17:325–31. [PubMed: 20400830]

Serduc R, et al. Synchrotron microbeam radiation therapy for rat brain tumor palliation—influence of the microbeam width at constant valley dose. Phys Med Biol. 2009a; 54:6711. [PubMed: 19841517]

Serduc R, Brauer-Krisch E, Bouchet A, Renaud L, Brochard T, Bravin A, Laissue JA, Le Duc G. First trial of spatial and temporal fractionations of the delivered dose using synchrotron microbeam radiation therapy. J Synchrotron Radiat. 2009b; 16:587–90. [PubMed: 19535875]

Serduc R, et al. Brain tumor vessel response to synchrotron microbeam radiation therapy: a short-term in vivo study. Phys Med Biol. 2008a; 53:3609–22. [PubMed: 18560052]

Serduc R, et al. Characterization and quantification of cerebral edema induced by synchrotron x-ray microbeam radiation therapy. Phys Med Biol. 2008b; 53:1153–66. [PubMed: 18296755]

Serduc R, et al. In vivo two-photon microscopy study of short-term effects of microbeam irradiation on normal mouse brain microvasculature. Int J Radiat Oncol Biol Phys. 2006; 64:1519–27. [PubMed: 16580502]

Shan, J.; Chtcheprov, P.; Tucker, AW.; Lee, YZ.; Wang, X.; Foos, D.; Heath, MD.; Lu, J.; Zhou, O. Stationary chest tomosynthesis using a CNT x-ray source array. In: Nishikawa, RM.; Whiting, BR., editors. Proc SPIE Medical Imaging Conference; Lake Buena Vista (Orlando Area), Florida, USA. 2013. p. 86680E

Slatkin DN, Spanne P, Dilmanian FA, Gebbers JO, Laissue JA. Subacute neuropathological effects of microplanar beams of x-rays from a synchrotron wiggler. Proc Natl Acad Sci USA. 1995; 92:8783–7. [PubMed: 7568017]

Slatkin DN, Spanne P, Dilmanian FA, Sandborg M. Microbeam radiation therapy. Med Phys. 1992; 19:1395–400. [PubMed: 1461201]

Smilowitz HM, et al. Synergy of gene-mediated immunoprophylaxis and microbeam radiation therapy for advanced intracerebral rat 9L gliosarcomas. J Neuro-Oncology. 2006; 78:135–43.

Thomlinson W, et al. Research at the European Synchrotron Radiation Facility medical beamline. Cell Mol Biol. 2000; 46:1053–63. [PubMed: 10976863]

Verhaegen F, Granton P, Tryggestad E. Small animal radiotherapy research platforms. Phys Med Biol. 2011; 56:R55–83. [PubMed: 21617291]

Van Hoof SJ, Granton PV, Landry G, Podesta M, Verhaegen F. Evaluation of a novel triple-channel radiochromic film analysis procedure using EBT2. Phys Med Biol. 2012; 57:4353–68. [PubMed: 22705890]

Winsor, L. Tissue processing. In: Woods, AE.; Ellis, RC., editors. Laboratory Histopathology. New York: Churchill Livingstone; 1994. p. 4.2-1-4.2-39.

Wong J, et al. High-resolution, small animal radiation research platform with X-ray tomographic guidance capabilities. Int J Radiat Oncol Biol Phys. 2008; 71:1591–9. [PubMed: 18640502]

Zeman W, Curtis HJ, Baker CP. Histopathologic effect of high-energy-particle microbeams on the visual cortex of the mouse brain. Radiat Res. 1961; 15:496–514. [PubMed: 14010109]

Zhang J, Yang G, C Y, Gao B, Qiu Q, Lee YZ, Lu J, Zhou O. Stationary scanning x-ray source based on carbon nanotube field emitters. Appl Phys Lett. 2005; 86:184104.

Zhong N, Morris GM, Bacarian T, Rosen EM, Dilmanian FA. Response of rat skin to high-dose unidirectional x-ray microbeams: a histological study. Radiat Res. 2003; 160:133–42. [PubMed: 12859223]

Zhou H, et al. Development of a micro-computed tomography-based image-guided conformal radiotherapy system for small animals. Int J Radiat Oncol Biol Phys. 2010; 78:297–305. [PubMed: 20395069]

Zhou, O.; Calderon-Colon, X. Carbon Nanotube-Based Field Emission X-Ray Technology. In: Saitō, Y., editor. Carbon Nanotube and Related Field Emitters. Vol. Chapter 26. Weinheim: Wiley-VCH; 2010. p. 417-37.

Zhou, OZ.; Chang, SX. Compact microbeam radiation therapy systems and methods for cancer treatment and research. U S patent. US2010/0329413 A1. 2010. Publication No

Zhou, OZ.; Lu, J. X-ray generating mechanism using electron field emission cathode. U S patent. 6,553,096 B1. 2003.

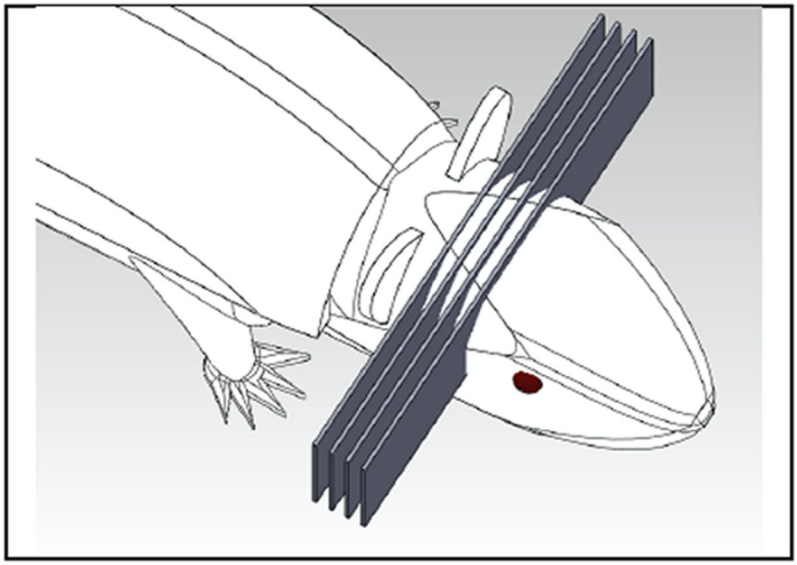

Figure 1.
SolidWorks (Dassault Systems, France) drawing of an array of microplanar beams traversing the mouse brain.

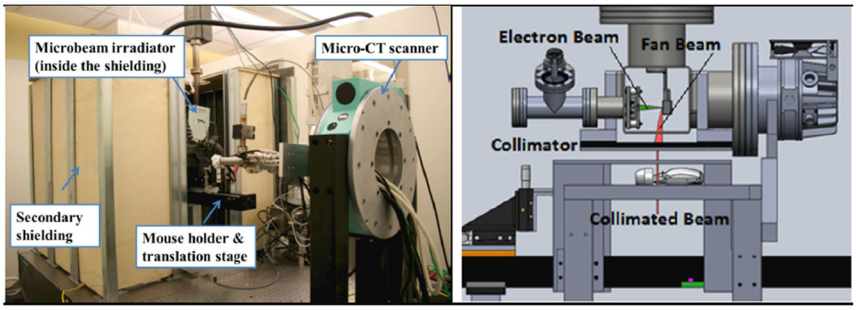

Figure 2.

Left: A photo of the irradiator surrounded by secondary shielding. Right: CAD drawing showing the detailed configuration of the microbeam radiation therapy system with the electron beam and X-ray beam indicated. The X-ray beam is collimated by a microbeam collimator to an adjustable beamwidth.

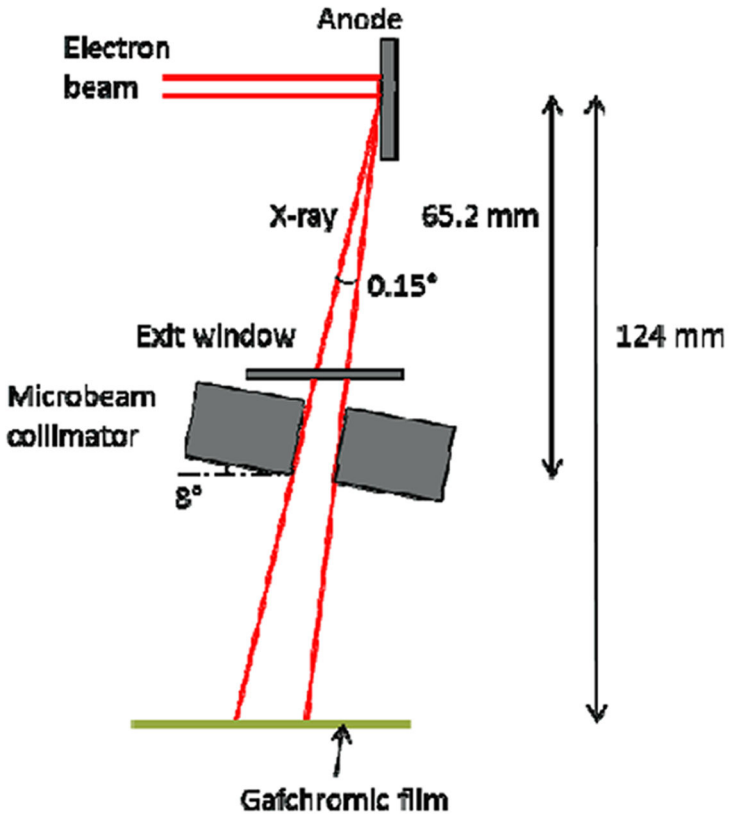

Figure 3.

Illustration of the geometry of our prototype MRT system and dose rate measurements. Dimensions were not drawn to scale. The effective focal line width on the anode after projection is approximately 142 μm in width and 160 mm in length. The microbeam collimator, made from two tungsten carbide parallels clamped against glass spacers, is at an 8 degree angle with respect to the anode surface, and the slit is 175 μm wide. The distance from the centre of focal line to the bottom of the collimator is about 65.2 mm. The divergence of the microplanar beam is around 0.15 degrees. For the dose rate measurement, a piece of Gafchromic film was irradiated at 124 mm from the focal line for different amounts of beam-on time.

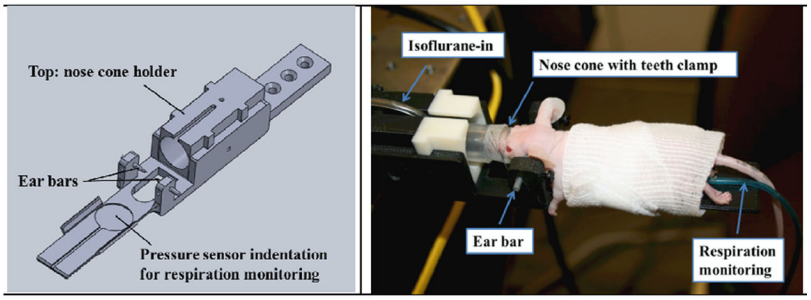

Figure 4.

Left: SolidWorks drawing of our customized mouse head holder with ear bars. The nose cone holder height can be adjusted based on the size and location of the mouse head. The nose cone can be moved forward and backward to get the isoflurane to the mouse during the irradiation. The pressure sensor is located underneath the abdomen of the mouse. Right: A picture of a mouse under anaesthesia immobilized on the holder with a piece of gauze wrapped around it to maintain its body temperature.

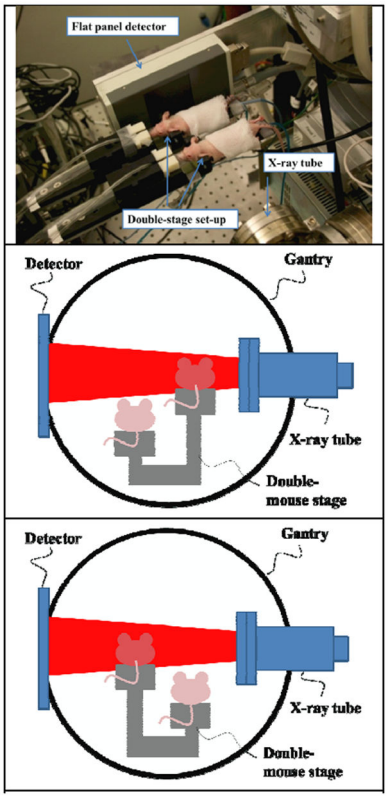

Figure 5.

A photo (top) and illustrations (middle and bottom) showing two mice imaged by X-ray scanner in the image-and-shift manner, with only one mouse in the FOV at a time. The double-stage enables vertical and horizontal adjustments.

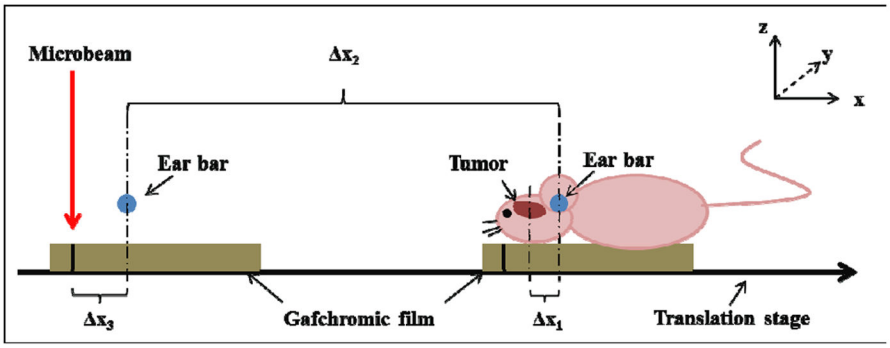

Figure 6.

Diagram showing the geometric relations between the targeted tumour, landmark, and microbeam locations. The y-direction is perpendicular to the paper plane. The microbeam plane is in the y-z plane. Δx_1 is the distance from the tumour to the ear bars measured in the registered image, Δx_2 is the distance of translation from the MRT chamber to the micro-CT, and Δx_3 is the distance between the centre of the ear bar and the alignment microbeam track measured during microbeam alignment. The mouse holder with the Gafchromic film was first irradiated for beam alignment, as shown on the left, and then translated to the right, followed by mouse positioning and X-ray imaging.

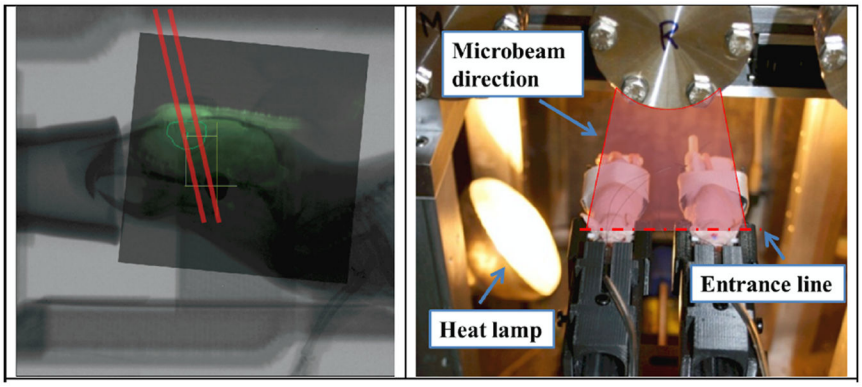

Figure 7.

Left: The registered image showed two microbeams (indicated by red lines) planned to ‘cut through’ the tumour region. The beam has a tilt of 8° from the collimator angle. Right: A photo of two mice irradiated together in the MRT chamber shown with the heat lamp on to maintain a certain body temperature during the radiation. The direction of the microbeam plane and the entrance point are also indicated.

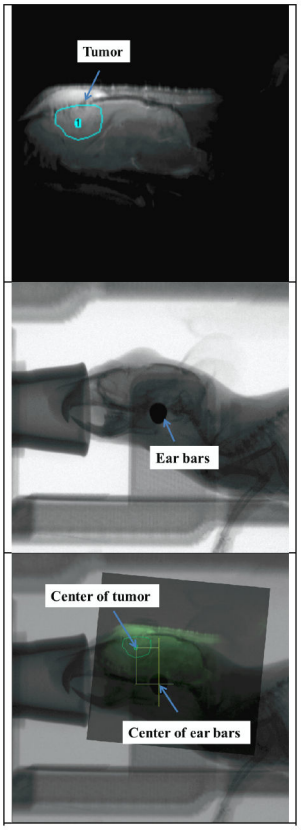

Figure 8.

Top: MR image of the mouse brain with the targeted tumour circled. Middle: X-ray projection of the same animal showing the landmark ear bars and skull features. Bottom: X-ray projection registered with MR image showing the relative position of the tumour and ear bars.

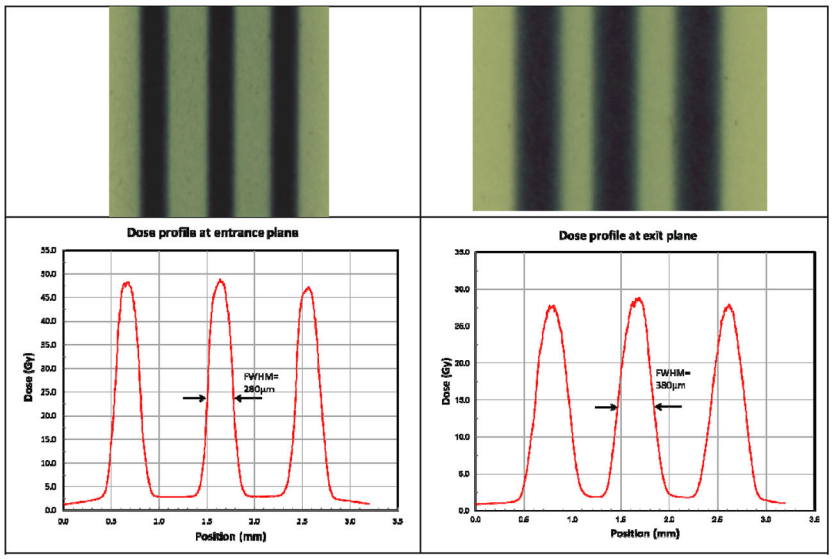

Figure 9.

Beam patterns recorded by *Gafchromic* films at the entrance (top left) and exit (top right) planes on the mouse head, and corresponding dose profiles (bottom) analyzed by *FilmQAPro* program (using multi-channel dosimetry). The beam width at the entrance plane is about 280 microns, and 380 microns at the exit plane. The PVDRs recorded for this animal were roughly 16 at the entrance plane, and 15 at the exit plane.

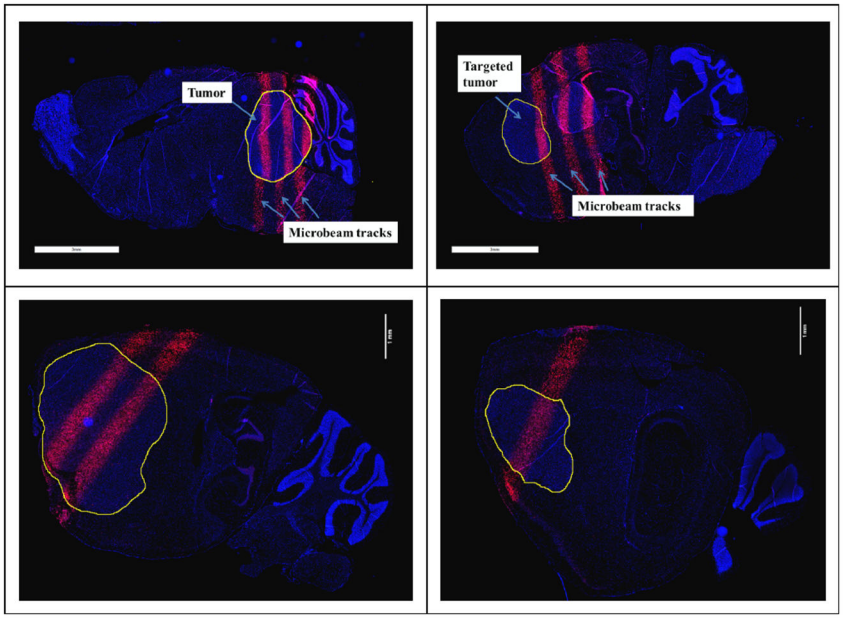

Figure 10.

γ-H2AX staining of the sliced brain tissue with three microbeams of 48 Gy/beam (top left and top right), two microbeams of 108 Gy/beam (bottom left), and a single microbeam of 138 Gy (bottom right). The images correspond to animal ID 1152 (top left), 1149 (top right), 1087 (bottom left), and 1089 (bottom right). The γ-H2AX foci-positive cells, shown as pink strips, correspond to the microbeam pattern. The circled areas are tumour sites.

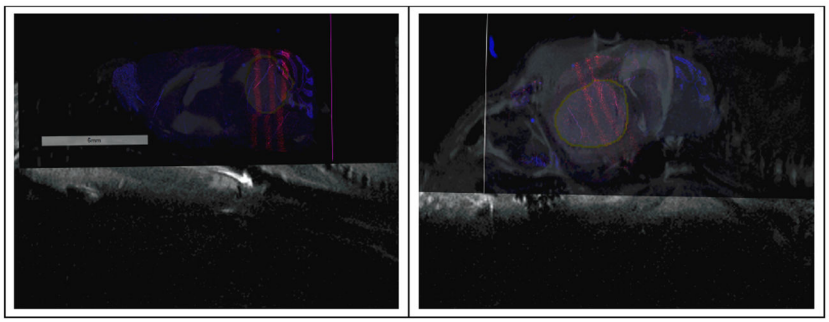

Figure 11.

γ-H2AX stained, sagittal image registered with MR projection for the same slice of tissue, from two animals (Left: ID 1152 and right: ID 1145) irradiated with three microbeams of 48 Gy/beam. Microbeam tracks are the pink strips through the higher contrast tumour region, demarcated by the yellow circle. The targeting error was measured from the microbeam location to the targeted tumour centre.

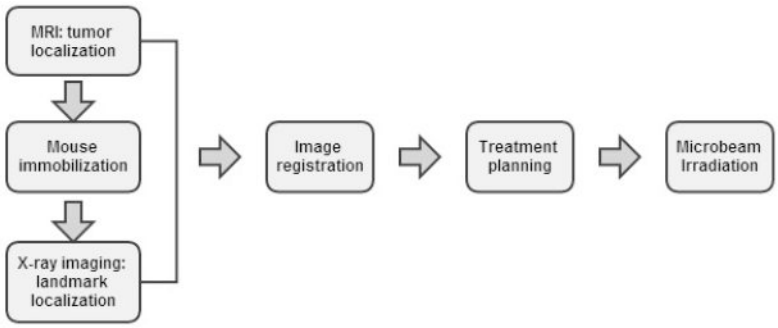

Chart 1.
MRI/X-ray radiograph combined image-guided MRT procedure.

Table 1

Summary of the targeting uncertainties.

Animal ID	Δx from staining-only (μm)	Δx from registered histological images (μm)	Number of MBs with peakentrance dose per beam
1087	290	390	Two beams, 108 Gy/beam
1086	800	1000	Single beam, 138 Gy/beam
1089	10	50	Single beam, 138 Gy/beam
1123	100	100	Three beams, 48 Gy/beam
1122	80	330	Three beams, 48 Gy/beam
1141	830	660	Three beams, 48 Gy/beam
1140	300	440	Three beams, 48 Gy/beam
1145	660	790	Three beams, 48 Gy/beam
1151	100	100	Three beams, 48 Gy/beam
1150	1130	1600	Three beams, 48 Gy/beam
1153	90	100	Three beams, 48 Gy/beam
1152	230	140	Three beams, 48 Gy/beam
1149	1280	1280	Three beams, 48 Gy/beam
Average	454	537	--
Standard Deviation	417	482	--